HHS Public Access

Author manuscript

J Mol Biol. Author manuscript; available in PMC 2017 October 09.

Published in final edited form as:

J Mol Biol. 2016 October 09; 428(20): 4031–4047. doi:10.1016/j.jmb.2016.07.018.

Phosphoinositide Binding Inhibits Actin Crosslinking and Polymerization by Palladin

Rahul Yadav, **Ravi Vattepu**, and **Moriah R. Beck**

Chemistry Department, Wichita State University, 1845 Fairmount Street, Wichita, KS 67260, USA

Abstract

Actin cytoskeleton remodeling requires the coordinated action of a large number of actin binding proteins that reorganize the actin cytoskeleton by promoting polymerization, stabilizing filaments, causing branching, or crosslinking filaments. Palladin is a key cytoskeletal actin binding protein whose normal function is to enable cell motility during development of tissues and organs of the embryo and in wound healing, but palladin is also responsible for regulating the ability of cancer cells to become invasive and metastatic. The membrane phosphoinositide phosphatidylinositol (PI) 4,5-bisphosphate [PI(4,5)P_2] is a well-known precursor for intracellular signaling and a bona fide regulator of actin cytoskeleton reorganization. Our results show that two palladin domains [immunoglobulin (Ig) 3 and 34] interact with the head group of PI(4,5)P_2 with moderate affinity (apparent K_d = 17 μM). Interactions with PI(4,5)P_2 decrease the actin polymerizing activity of Ig domain 3 of palladin (Palld-Ig3). Furthermore, NMR titration and docking studies show that residues K38 and K51, which are present on the β-sheet C and D, form salt bridges with the head group of PI(4,5)P_2. Moreover, charge neutralization at lysine 38 in the Palld-Ig3 domain severely limits the actin polymerizing and bundling activity of Palld-Ig3. Our results provide biochemical proof that PI(4,5)P_2 functions as a moderator of palladin activity and have also identified residues directly involved in the crosslinking activity of palladin.

Keywords

phospholipid; actin cytoskeleton; regulation; electrostatics; NMR

Introduction

The membrane phosphoinositide, phosphatidylinositol (PI) 4,5-bisphosphate [PI(4,5)P_2], plays a fundamental role in membrane-associated cellular processes such as cytokinesis [1], intracellular signaling [2], vesicle trafficking [3], and restructuring of the cellular cytoskeleton [4]. PI(4,5)P_2 is concentrated on the cytosolic face of the plasma membrane and accounts for less than 1% of the total cellular pool of lipids [4,5]. In particular, PI(4,5)P_2 plays an important role in actin cytoskeleton remodeling by directly interacting with and controlling subcellular localization of several actin binding proteins (ABPs) both spatially

Correspondence to Moriah R. Beck: moriah.beck@wichita.edu.

Present address: R. Yadav, Department of Medicinal Chemistry, University of Kansas, Lawrence, KS 66045, USA.

Edited by M.F. Summers

and temporally. For instance, $PI(4,5)P_2$ promotes actin polymerization near the cell membrane by activating the actin nucleating and branching protein actin-related protein-2/3 complex via activation of N-WASP [6] and/or by blocking the barbed-end capping activity of gelsolin [7,8]. $PI(4,5)P_2$ also downregulates the activity of filamin and α-actinin and thereby decreases cross-linking of filamentous actin (F-actin) [9,10]. $PI(4,5)P_2$ can also upregulate adhesion by inducing conformational changes in otherwise autoinhibited actin cross-linking proteins vinculin and talin [11]. Moreover, reduced cellular concentrations of $PI(4,5)P_2$ result in the loss of cytoskeleton adhesion from cell membranes [12]. In general, the phosphoinositol head group mediates the interaction of $PI(4,5)P_2$ with ABPs, which is facilitated by electrostatic interactions between the negatively charged lipid head group and the positively charged basic amino acids of the protein. However, in some cases, the acyl chain of $PI(4,5)P_2$ also facilitates this interaction with proteins [13]. Moreover, some ABPs are indiscriminate in recognizing other phosphoinositides {PI, PI 4-phosphate [PI(4)P], PI 3,4-bisphosphate [$PI(3,4)P_2$], and PI 3,4,5-trisphosphate}. For example, $PI(4,5)P_2$ is capable of inhibiting the actin depolymerization activity of cofilin proteins in chicken and yeast, yet cofilin can likewise bind to $PI(3,4)P_2$ and PI 3,4,5-trisphosphate with relatively high affinity [13,14]. These diverse actions highlight the broad scope of $PI(4,5)P_2$ activities in reorganizing the actin cytoskeleton.

Palladin, a cytoskeletal ABP, is widely expressed in muscle and non-muscle cells of vertebrates [15]. It has been functionally linked to the regulation of actin dynamics in normal embryonic development [16], wound healing [17,18] and invasive cancers [19,20]. Suppression of palladin expression results in the loss of stress fibers in fibroblasts cells [21], decrease in the amount of F-actin [22], defects in cell motility through reduced expression of contractile proteins [23], and loss of cytoskeletal organization. Conversely, overexpression of palladin in cultured cells increases the number and size of actin bundles [24].

Palladin is a multi-domain scaffolding protein that also interacts directly with actin and crosslinks actin filaments [25,26]. Its scaffolding activity regulates actin dynamics via interactions with other actin binding and crosslinking proteins, such as ENA/vasodilator-stimulated phosphoprotein [27], profilin [28], α-actinin [29], Lasp-1 [24], and Ezrin [15]. Moreover, palladin interacts with signaling intermediates (Src, SPIN-90, and Abl/Arg kinase binding protein) that are associated with cytoskeletal reorganization [30,31]. The largest isoform of palladin (isoform #1, ~200 kDa) contains five immunoglobulin (Ig) domains: two amino terminal Ig domains (Ig1, Ig2), followed by two polyproline-rich regions and three C-terminal Ig domains (Ig3–Ig5) [32,33]. The Ig domain 3 of palladin (Palld-Ig3) has been shown to be both necessary and sufficient for both actin binding and crosslinking [25,26,34]. Despite the fact that the Ig4 domain and the linker between the Ig3 and Ig4 domains of palladin do not interact directly with actin, their addition increases actin binding and crosslinking activity significantly over that of the Ig3 domain alone [35]. Two lysine patches (K15/18 and K51) on the surface of Palld-Ig3 have been implicated directly in its actin binding activity, and it was suggested initially that these sites are also involved in its actin crosslinking activity [26]. Vattepu *et al.* (2015) have shown that actin crosslinking is the result of actin-induced homodimerization of the Palld-Ig3 domain [35]; however, the residues of Palld-Ig3 involved in homodimerization have not yet been identified.

Our lab has recently shown that palladin can increase the rate of actin polymerization and also alters the organization of the resulting filaments [34]. Moreover, removal of the actin binding domain (Palld-Ig3) results in the relocation of palladin to the nucleus [26], suggesting that direct binding with actin has major implications for palladin's role in cytoskeletal reorganization. Palladin also binds numerous cellular components other than F-actin, including multiple other ABPs, signaling intermediates, and transcription factors. Many of these binding partners regulate actin assembly; thus, palladin resides at the center of a complex network to organize actin architecture. Therefore, it is crucial to understand the mechanisms through which the interactions in this network are regulated. Despite its well-established role in normal and invasive cell motility, regulation of palladin remains unexplored.

Here, we have determined the functional regulation of palladin by anionic membrane phospholipids. We show that $PI(4,5)P_2$ directly interacts with the actin binding domain of palladin (Palld-Ig3). The Palld-Ig3 interaction with $PI(4,5)P_2$ appears to be electrostatic in nature, which also drives weaker interactions with PI, PI(4)P and inositol trisphosphate [$Ins(1,4,5)P_3$]. Functionally, binding of $PI(4,5)P_2$ to Palld-Ig3 decreases its crosslinking activity and *de novo* actin filament assembly without significantly affecting actin binding. We have also identified the potential $PI(4,5)P_2$-interacting residues on the Palld-Ig3 domain. Interestingly, these interactions involve two lysine residues that do not have any significant effect on actin binding and lie on the face opposite to that of one of the known actin binding sites. While mutation of these sites did not affect the actin binding activity, the actin crosslinking activity and the rate of actin polymerization by Palld-Ig3 are both significantly decreased. Together, these results suggest that $PI(4,5)P_2$ is a potent regulator of palladin that interferes with actin crosslinking.

Results

Palld-Ig3/Ig34 domains interact with $PI(4,5)P_2$-enriched liposomes

As a preliminary experiment to determine the interaction of $PI(4,5)P_2$ with palladin domains (Palld-Ig3, 4, or 34), we used the well-established liposome co-sedimentation assay [36–38]. In liposome co-sedimentation assays, the amount of protein bound to liposomes was examined by using a constant concentration of Palld-Ig3/4/34 (10 μM) while varying the $PI(4,5)P_2$ concentration (5–20%) in 1-palmitoyl-2-oleoyl-sn-glycero-3-phosphocholine (POPC) vesicles (95–80%). We observed significant co-pelleting of both Palld-Ig3 and Ig34 with increasing concentrations of $PI(4,5)P_2$ in POPC vesicles (Fig. 1a and b). Although Palld-Ig4 showed some increase in sedimentation at higher $PI(4,5)P_2$ concentrations (15–20%), the pelleted amount was significantly lower than Palld-Ig3 or Ig34. Moreover, Palld-Ig34 showed significantly more co-sedimentation ($P < 0.0001$) than Palld-Ig3 ($P < 0.0014$) at all $PI(4,5)P_2$ concentrations and nearly all of the Palld-Ig34 pelleted at higher concentrations of $PI(4,5)P_2$ (15–20%). Co-sedimentation of these individual palladin domains with only POPC vesicles produced minimum sedimentation of proteins in comparison to POPC:$PI(4,5)P_2$ vesicles; however, co-sedimentation of Palld-Ig34 is greater than that for Palld-Ig3 or Ig4 with POPC vesicles. Importantly, co-sedimentation of palladin domains increased significantly with increasing concentrations of $PI(4,5)P_2$ in the vesicles.

Electrostatic interaction mediates PI(4,5)P_2 interaction with Palld-Ig3/34

The next set of experiments was carried out to determine whether interactions between Palld-Ig3 and Ig34 with PI(4,5)P_2 are dependent on the charge of the head group of anionic PI and whether other anionic membrane phospholipids have any propensity to interact with Palld-Ig3 and Ig34. Vesicle co-sedimentation assays were repeated with vesicles prepared by mixing POPC with 15% PI, PI(4)P, or PI(4,5)P_2. These phospholipids (PI) differ in their subcellular distribution and the charge on their head group. PI, PI(4)P, and PI(4,5)P_2 carry net charges of −1, −2, and −3, respectively [39]. Although some phospholipid binding proteins can discriminate between different phosphoinositides [PI(4,5)P_2, PI(3,4)P_2, and PI(3,5)P_2] in *in vitro* binding assays, the cellular concentration and membrane distribution of these phosphoinositides ensure *in vivo* binding specificity. As the most abundant phosphorylated phsophoinositide, PI(4,5)P_2 represents ~1–2% of the total pool of cellular phospholipids and is distributed asymmetrically to the inner leaflet of the plasma membrane [4]. Yet, PI(3,4)P_2, which is also present in the inner leaflet of the plasma membrane, has a concentration that is 100-fold lower than that of PI(4,5)P_2 (at 2–5% of total phosphoinositde pool). While PI(3,5)P_2 carries net negative charges similar to that of PI(4,5)P_2, it is localized almost entirely to the late endosomes and comprises only <0.05% of total phosphoinositides in mammalian cells [40].

We observed significant co-sedimentation of Palld-Ig3 and Ig34 with these vesicles; however, the amount of pelleted protein increased with the order of PI < PI(4)P < PI(4,5)P_2 (Fig. 1c and d). This suggests that phospholipid binding by Palld-Ig3 and Ig34 increases with increasing charge on the head group and is indicative of an electrostatically driven interaction between the negatively charged head group of PIs and the positively charged amino acids of Palld-Ig3.

The interaction of vesicles of different lipid compositions with Palld-Ig3 was further investigated by monitoring the changes in the NMR signal upon titration with increasing amounts of phospholipids [41,42]. As shown in Supplementary Fig. 6, small signal losses were observed upon titration of Palld-Ig3 with liposomes containing PC; however, PC liposomes containing increasing amounts of PI(4,5)P_2 resulted in significantly increased signal attenuation, indicating that PI(4,5)P_2 enhances the affinity of palladin for liposomes. A more moderate effect was measured for PI(4)P-containing liposomes, and PS promoted even less effective binding at similar concentrations. This result clearly indicates that the perturbation is increased with increasing amounts of negatively charged lipids.

Quenching of intrinsic tryptophan fluorescence by PI(4,5)P_2

Intrinsic tryptophan quenching assays were performed next to further characterize the interaction of PI(4,5)P_2 with palladin domains. Tryptophan quenching was previously employed to measure PI(4,5)P_2 binding to several other ABPs [43–45]. The fact that most Ig domains have a single tryptophan in the hydrophobic core, including the Ig3 and Ig4 domains of palladin [46], facilitates the use of tryptophan quenching studies. In this assay, PI(4,5)P_2 was serially added to the protein solution, and the fluorescence signal was recorded. We did not detect any red or blue shift in the position of emission maxima wavelength, which remained essentially around 330 nm for all three domains, suggesting

that the addition of $PI(4,5)P_2$ does not affect the structural integrity of the palladin domains. Similar to the results obtained in our vesicle co-sedimentation assay, maximum quenching of tryptophan fluorescence was observed for both the Palld-Ig3 and Ig34 domains upon addition of $PI(4,5)P_2$ (Fig. 2a and c), whereas no significant change in the intensity was observed for Palld-Ig4 (Fig. 2d). We analyzed fluorescence quenching data as a function of $PI(4,5)P_2$ concentration to determine the binding affinity of Palld-Ig3 and Ig34 with $PI(4,5)P_2$ by fitting the respective values in Eq. (1), which yielded a dissociation constant (K_d) of 17.3 ± 2.1 and 13.5 ±4 μM, respectively (Fig. 2b). Titration of $PI(4,5)P_2$ in Palld-Ig34 resulted in fluorescence quenching akin to the titration of $PI(4,5)P_2$ in Palld-Ig3, albeit with higher SD. Yet, the overall trend remained similar in all three repetitions for Palld-Ig34. A similar assay was carried out to ascertain the effect of POPC on palladin domains, and we observed minimal tryptophan quenching for all three proteins in comparison to the results obtained for $PI(4,5)P_2$ titration (Supplementary Fig. 1); however, we did detect some minor differences in the extent of quenching. Here, the most significant quenching occurred for Palld-Ig34, followed by Ig3 and Ig4, and this trend mirrored the results we obtained in the POPC vesicle co-sedimentation assay. POPC, although zwitterionic, displays only a slightly negatively charged behavior in salt solutions, which has been attributed to the binding of anion to the trimethylammonium group of the POPC lipid [47,48]. This propensity to carry a net negative charge by POPC lipids is a likely explanation for the minimal binding to palladin domains that leads to some measurable co-sedimentation and tryptophan quenching in our assays. Together, these results suggest that while Palld-Ig4 has very minor affinity for $PI(4,5)P_2$, the primary $PI(4,5)P_2$ binding activity resides in the actin binding domain of palladin (Palld-Ig3).

Binding of $PI(4,5)P_2$ decreases actin crosslinking and polymerizing activity of palladin

Dixon *et al.* (2008) have shown that both Palld-Ig3 and Ig34 can bind to F-actin and that the actin binding activity of palladin resides mainly within the Ig3 domain [25]. Although the Ig4 domain and the intervening linker between the Ig3 and Ig4 domains of palladin have not shown any direct interaction with actin [25], the actin binding and crosslinking activity of the tandem Ig34 domain are both significantly greater than the isolated Palld-Ig3 domain [25,26]. Recognizing that the Ig3 domain is the minimal structural unit of palladin that is sufficient for actin binding and crosslinking, we wanted to know the functional significance of $PI(4,5)P_2$ interaction with this domain. First, we performed conventional actin binding co-sedimentation assay with F-actin and Palld-Ig3 in the presence of varying concentrations of $PI(4,5)P_2$. This assay revealed that the addition of $PI(4,5)P_2$ has minimal effect on the actin binding activity of Palld-Ig3 (Supplementary Fig. 2). Therefore, we next investigated the effect of $PI(4,5)P_2$ on the actin crosslinking activity of Palld-Ig3. We chose non-polymerizing conditions because the actin crosslinkng activity of Palld-Ig3 is significantly higher as a result of co-polymerization with actin, as opposed to the addition of Palld-Ig3 to pre-polymerized actin filaments [34]. We observed a significant decrease in actin crosslinking [15–40% with $PI(4,5)P_2$ as opposed to 60% without $PI(4,5)P_2$] in a dose-dependent manner upon the addition of varying concentrations of $PI(4,5)P_2$ mixed with Palld-Ig3 and globular or monomeric actin (G-actin) (Fig. 3a and b). The fact that $PI(4,5)P_2$ reduces the actin crosslinking activity of Palld-Ig3, without significantly altering its actin

binding activity, suggests that the actin binding and crosslinking sites on Palld-Ig3 are structurally independent.

Recently, we have shown that the Palld-Ig3 domain also promotes *de novo* actin nucleation and polymerization [34]. Therefore, we next sought to determine whether PI(4,5)P_2 binding has any effect on palladin's actin nucleation and polymerization activity. Consequently, we first used an actin co-sedimentation assay with the modification and we initiate the reaction with G-actin, instead of F-actin, and strictly avoid any polymerization-inducing cations (K^+ and Mg^{2+}). Moreover, we have added 1 mM ethylene glycol tetraacetic acid (EGTA) to the G-actin and G-buffer just prior to the experiment to chelate any calcium, which could lead to aggregation of PI(4,5)P_2. Most of the G-actin is polymerized and is found in high-speed pellets in the control sample [without PI(4,5)P_2] for both Ig3 and Ig34 (Fig. 3c, first lanes); however, we detected an increasing amount of G-actin in the supernatant fraction upon co-incubation of G-actin with a complex of PI(4,5)P_2 (50–150 μM) and Palld-Ig3 or Ig34 in G-buffer conditions. Likewise, less palladin was co-pelleted with actin with increasing concentrations of PI(4,5)P_2 (Fig. 3c and d). As much as 50% decrease in the actin polymerization was observed at the highest concentration of PI(4,5)P_2 (Fig. 3d). Moreover, chelation of calcium from the G-actin did not alter the actin nucleation and polymerization activity of palladin, which is in agreement with the mechanism proposed by Gurung *et al.* (2016), whereby the binding of Palld-Ig3 to actin transforms G-actin to nucleation- and polymerization-competent form through charge neutralization or conformational change [34].

Next, we monitored the effect of PI(4,5)P_2 on the rate of F-actin assembly as promoted by Palld-Ig3/Ig34 in a bulk solution assay that takes advantage of the fact that the fluorescence intensity of pyrenyl-G-actin increases 7- to10-fold upon polymerization, which is directly proportional to the amount of G-actin incorporated into F-actin [49]. We measured the complete time course of actin polymerization, using 5 μM G-actin and 20 μM Palld-Ig3 or 10 μM Ig34 in the presence of varying concentrations of PI(4,5)P_2 (0–100 μM) under polymerizing and non-polymerizing conditions. We observed a decrease in actin polymerization with increasing concentrations of PI(4,5)P_2 in both Palld-Ig3 and Ig34 in F-buffer conditions (Fig. 4a and b). Moreover, a lag phase that is characteristic of a slow nucleation step in actin polymerization was observed at higher concentrations of PI(4,5)P_2. A similar trend for actin polymerization by Palld-Ig3 in the presence of PI(4,5)P_2 was observed in non-polymerizing conditions (Supplementary Fig. 3). Similar experiments with Palld-Ig34 in non-polymerizing conditions could not be monitored accurately due to the extremely fast polymerization rate, which could not be resolved well at initial time points. Importantly, we observed a significant decrease in the rate of actin polymerization promoted by Palld-Ig3 or Ig34 with increasing concentrations of PI(4,5)P_2. Moreover, the rate of actin polymerization was found to be twofold higher for Palld-Ig34 (15 nM/s) than for Palld-Ig3 (7 nM/s) at saturating concentrations of these proteins (Fig. 4c). This difference likely reflects the fact that Palld-Ig34 has a greater, apparent actin-binding affinity (K_d = ~9 μM), which is closer to that of full-length palladin (K_d = ~2.1 μM) than Ig3 (K_d = ~60 μM) [25].

Mapping of inositol 1,4,5-triphosphate-induced chemical shift change

To define the nature and specific binding site for PI(4,5)P_2 on Palld-Ig3, we have collected a pair of ^{1}H–^{15}N heteronuclear single quantum correlation spectroscopy (HSQC) spectra of Palld-Ig3 (0.2 mM) with or without saturating concentrations (1 mM) of Ins(1,4,5)P_3 [i.e., head group of PI(4,5)P_2]. Since we were interested in the specific interaction of the PI(4,5)P_2 head group without any interference by the acyl tail of PI(4,5)P_2, we consciously choose to collect NMR spectra with Ins(1,4,5)P_3. However, we did observe significant chemical shift perturbations (CSPs; >0.04 ppm) for a cluster of residues on the Palld-Ig3 domain: K38, I39, W41, F42, Q47, S49, K51, and I57 (Fig. 5). In addition, we detected few residues (F9, T64, H68, and N86) that were spatially separated from the first cluster of residues but display significant chemical shift changes upon titration of Ins(1,4,5)P_3 (Fig. 5b). Mapping these signifiantly perturbed residues onto the solution structure of Palld-Ig3 (PDB ID: 2LQR) reveals that the most perturbed residues lie at the interface between β-strands C and D and the loop between these strands (Fig. 6a and b). Interestingly, these residues are located on the face opposite to that of the known actin binding site (K15 and K18) [26]. The only tryptophan (W41) present in the Palld-Ig3 domain, which is partially buried in the hydrophobic core, shows strong chemical shift deviations in the presence of Ins(1,4,5)P_3. This strong CSP substantiates the previously observed tryptophan quenching results and indicates that W41 resides near the PI(4,5)P_2 binding site. We infer from the CSP result that two surface-exposed lysines (38 and 51) might play an important role in Ins(1,4,5)P_3 interactions. Decreased actin binding and crosslinking activity have been associated with the mutation of one of these lysine residues (K51A) [26]. However, a similar mutation K38A in Palld-Ig3 did not affect actin binding in previous actin co-sedimentation assays [26]. The exposure of strong CSPs for both K38 and K51 upon Ins(1,4,5)P_3 titration suggests that electrostatics is an important determinant for palladin's interactions with Ins(1,4,5)P_3, reminiscent of palladin's interactions with actin.

Molecular docking of Ins(1,4,5)P_3 onto the Palld-Ig3 structure

The polar head group of PI(4,5)P_2 [Ins(1,4,5)P_3] was used for docking studies aimed at identifying the sites of interaction between Palld-Ig3 and PI(4,5)P_2. The docking procedure was initiated with the NMR structure of Palld-Ig3 domain (PDB ID: 2LQR) [26] and Ins(1,4,5)P_3 (PDB ID: 1N4K) as starting coordinates using the guru interface of High Ambiguity Driven protein–protein DOCKing (HADDOCK2.2) [50]. Rigid-body docking with flexible side chains of Palld-Ig3 and Ins(1,4,5)P_3 resulted in a total of 198 water-refined conformers in three clusters. The cluster with the lowest HADDOCK score (−114.6 ± −3.2 kCal/mol) contained 175 conformers with an RMSD of 0.5 from the lowest energy structure. Examination of the best representative conformer from the cluster suggests that the Ins(1,4,5)P_3 molecule binds at the concave side formed between β-strand C and D via basic residues from the β-strand C and the following loop (K38 and K51). The Ins(1,4,5)P_3 molecule interacts with Palld-Ig3 via a salt bridge between side chains of K38, Q47, S49, K51, R59 and inositol phosphates (Fig. 6c and d).

Lysine mutation of K38/51A decreases the actin crosslinking substantially

A previous study revealed that alanine substitutions of lysine 38 in Palld-Ig3 had only minor or no effect on actin binding, while mutation of lysine 51 resulted in a 10% decrease in binding in comparison to wild-type (WT) Palld-Ig3 [26]. Identification of these residues as the likely lipid binding site from docking studies prompted us to revisit the actin binding assay with a Palld-Ig3-K38/51A double-mutant protein. We observed that ~30% of WT Palld-Ig3 co-sediments with F-actin at and above saturating concentrations, which was similar to the previously published data [26]. However, actin binding for Palld-Ig3 K38/51A mutant only reached 20–22% at saturating concentrations in similar reaction conditions as for WT Palld-Ig3 (Fig. 7a and Supplementary Fig. 4A). While this decrease in actin binding for the K38/51A mutant is minor, it may be significant in terms of highlighting a potential secondary actin binding site that could facilitate the crosslinking of F-actin. In the previous study by Beck *et al.* (2014), an actin crosslinking model was proposed in which two basic patches are involved in actin binding, namely, one involving lysine15 and 18 and a second located at lysine 51 on the opposite face of Palld-Ig3 [26]. Both lysines 38 and 51 are located on the face opposite of lysines 15 and 18; thus, our results suggest that K51 is joined by K38 to form a cluster of lysine residues that is involved in actin binding and/or bundling.

Therefore, we next examined the actin crosslinking activity of the K38/51A Palld-Ig3 mutant. We chose non-polymerizing conditions for this assay similar to that of Palld-Ig3 actin crosslinking in the presence of $PI(4,5)P_2$. In this co-polymerization bundling assay, crosslinking by Palld-Ig3-K38/51A was dramatically decreased to approximately 5–15% as opposed to 70% for WT Palld-Ig3 (Fig. 7b and Supplementary Fig. 4B). Moreover, a significant fraction of actin remained monomeric when incubated with mutant Palld-Ig3, suggesting that this mutation also affects the polymerizing activity. Therefore, we have identified the lysine residues (K38 and K51) in the actin binding domain of palladin that affect actin cross-linking to a much greater degree than actin binding. This finding will be useful in teasing apart the two separate roles for palladin in actin binding *versus* crosslinking.

To monitor the effect of these mutations on the rate of actin polymerization, we repeated the actin polymerization kinetic assay with Palld-Ig3-K38/51A (Supplementary Fig. 5B). In contrast to our previous experiments invovling $PI(4,5)P_2$:Palld-Ig3 complexes, we used a priming solution here (0.1 mM $MgCl_2$ and 1 mM EGTA) to convert to Mg-actin just prior to each assay. The K38/51A mutant took twice as long as WT Palld-Ig3 to reach the plateau (Supplementary Fig. 5). Moreover, polymerization of actin exhibited a lag phase even at higher concentrations of Palld-Ig3 K38/51A, suggesting a minimal effect on the rate of actin polymerization.

Discussion

Previous studies have demonstrated the role of palladin as a cytoskeletal scaffold and an actin crosslinking protein. Recently, our group has shown that Palld-Ig3 is capable of *de novo* actin nucleation by promoting the G➔G* transition of G–actin, leading to an increased rate of actin polymerization and stabilization of actin filaments [34]. This previous work has provided causative links between overexpression of palladin and altered

cytoskeletal dynamics that lead to the formation of invadopodia required for metastasis of cancer cells [20,34,51]. However, the mechanism for regulating the actin binding activity of palladin is not well understood. Several studies of ABPs have illustrated that surface-exposed and positively charged residues facilitate interactions with actin, which has also been found true in the case of paladin [26]. Previous studies have also shown that some acidic phosphoinositides, such as $PI(4,5)P_2$, can mask or expose actin binding sites and thereby modulate the actin dynamics essential to cell surface events [4]. In this study, we report that membrane phosphoinositide $PI(4,5)P_2$ interacts with the actin binding domain of palladin with moderate affinity and also diminishes the actin polymerization activity of palladin. Moreover, we have also identified two lysine residues (K38 and K51) in the actin binding domain of palladin that do not significantly affect actin binding but notably reduce the actin crosslinking activity.

Our data show that the Ig3 and Ig34 domains of palladin bind to acidic phospholipids under physiological conditions, whereas the isolated Ig4 domain did not show significant co-sedimentation in similar experimental conditions. Interestingly, while Palld-Ig4 binding to POPC:$PI(4,5)P_2$ liposomes was minimal, a much higher degree of $PI(4,5)P_2$ co-sedimentation was observed for the tandem Palld-Ig34 compared to that for Palld-Ig3 alone. This enhancement is similar to the previous reports for actin binding of Palld-Ig3 as compared to Ig34 [25]. While the isolated domain of Palld-Ig4 does not bind directly to actin, this isolated domain does enhance the actin binding and cross-linking activity of Palld-Ig3 when present as the tandem domain (Palld-Ig34) [25]. Although the mechanism governing this phenomenon has not been fully uncovered, a previous study by Vattepu *et al.* (2014) suggested that actin binding stabilizes palladin homodimers, which in turn enhances actin binding and crosslinking [35]. A similar mechanism for the enhanced co-sedimentation of Palld-Ig34 with POPC:$PI(4,5)P_2$ cannot be resolved at this point; however, it is quite likely that the weak interaction of Palld-Ig4 with POPC:$PI(4,5)P_2$ or of Palld-Ig34 with POPC contributes to the enhanced co-sedimentation.

As part of our analysis, we determined the dissociation constant, K_d, for Palld-Ig3 and $PI(4,5)P_2$ using a tryptophan quenching assay. We determined that $PI(4,5)P_2$ interacts with Palld-Ig3 with moderate affinity (K_d = ~17 μM), which is similar to $PI(4,5)P_2$ binding affinities reported for gelsolin (40 μM), CapG (32 μM), and vilin (39.4 μμ) from similar fluorescence quenching assays [43,52]. While the isolated Ig3 domain of palladin displays similar binding affinities for both actin (60 μM) and $PI(4,5)P_2$ (~17 μM), the binding affinities of full-length palladin and Palld-Ig34 for actin are both stronger (K_d = ~2 μM and ~9 μM, respectively), which represent the binding affinity of palladin for actin [25]. Both the nonhomogeneous distribution and discrete clustering of $PI(4,5)P_2$ in the cell membrane affect the local concentration of $PI(4,5)P_2$ *in vivo* [53], which in turn can modulate the interaction of lipid-binding proteins. Therefore, the competing interaction between palladin and actin may not preclude its interaction with $PI(4,5)P_2$ in dense regions of this phospholipid in the cell membrane environment. Although there is no direct evidence for $PI(4,5)P_2$ interactions with palladin *in vivo*, plenty of indirect evidence supports this interaction. In general, it is well established that palladin localizes at the cell membrane and is involved in communication with various forms of external stimuli. Palladin co-localizes with bundles of actin filaments at dorsal stress fibers that are distributed throughout the

cytoplasm, but palladin is also found at sites that are associated with the plasma membrane, where cells form connections to the extracellular matrix (ECM) or cell–cell association, such as membrane ruffles, podosomes, and invadapodia [53]. Recent work from von Nandelstadh *et al.* (2014) has demonstrated that the C-terminal domain of palladin (Ig345) interacts with the intracellular domain of membrane type 1 matrix metalloproteinase at ECM adhesion sites and promotes ECM degradation [54]. Moreover, it has been shown that palladin maintains the structural integrity of lamellipodia and focal adhesions [22]. Palladin also cooperates with lipoma partner protein at focal adhesions [55]. This growing list of membrane-associated functions and partners suggests that palladin belongs to the class of proteins that connects adhesion molecules in the cell membrane to the cytoskeleton and indicates an important functional role for phospholipid binding by palladin.

While previous work has established that the Ig3 domain of palladin promotes actin crosslinking and polymerization, we show here that interactions with $PI(4,5)P_2$ affect both activities. On one hand, $PI(4,5)P_2$ decreases actin crosslinking and polymerization by palladin. This is in contrast to the observation that $PI(4,5)P_2$ did not affect actin binding by Ig3 in polymerizing conditions (F-buffer). This dichotomy can be explained by highlighting the fact that actin binding requires only one binding site; however, crosslinking and polymerization likely involve multiple interactions and/or conformational changes in palladin, such as actin-induced dimerization [35]. Our previous work indicated that Palld-Ig3 stimulates actin nucleation and polymerization and that the crosslinking of actin filaments that occurs during polymerization is far greater than the bundling of pre-formed actin filaments [34]. Here, we observe an obvious decrease in actin crosslinking by palladin upon binding to $PI(4,5)P_2$, which correlates with decreases in actin polymerization. Moreover, our current study clearly indicates that Palld-Ig34 is at least four times more efficient than Palld-Ig3 in stimulating *de novo* actin nucleation and polymerization. This claim is based on the fact that the rate of polymerization is increased by a factor of 2 for half of the concentration of Palld-Ig34, as compared to Ig3 (Fig. 4c). The steady-state plateau in fluorescence signal intensity reached by the tandem Ig34 domain is more than double for the single domain and reaches this concentration of polymerized actin more rapidly and at a lower concentration of Palld-Ig34 in similar experimental conditions. This combination of factors suggests that Palld-Ig34 is much more effective than Palld-Ig3 in promoting and stabilizing actin polymerization and is therefore a better model for *in vitro* studies, where the highly unstable, full-length palladin protein cannot be used.

Our results suggest that electrostatic interactions between $PI(4,5)P_2$ and Palld-Ig3 or Ig34 are critical. Using NMR, we have identified a cluster of residues (K38, I39, W41, F42, Q47, S49, K51, and I57) on the Ig3 domain of palladin that represent the putative $PI(4,5)P_2$ and $Ins(1,4,5)P_3$ binding sites. Moreover, docking of $Ins(1,4,5)P_3$ onto the structure of Palld-Ig3 substantiates the involvement of residues K38 and K51 in this interaction. Correlation of tryptophan fluorescence quenching upon the addition of $PI(4,5)\ P_2$ and the significant CSP observed for W41 in Palld-Ig3:$Ins(1,4,5)P_3$ suggests that $PI(4,5)P_2$ and $Ins(1,4,5)P_3$ share a binding region on Palld-Ig3. A similar phosphoinositide binding motif has been identified in a group of ABPs that consists of a series of positively charged amino acids in the following arrangement: R/K-$(X)_4$-[R/K]-X-[RR/KK] [52,56]. Sequence comparison of Palld-Ig3 with this phosphoinositide binding motif reveals that at least three charged residues are conserved

in the lipid binding region of Palld-Ig3, between residues K38 to K46 (Fig. 8). In fact, palladin contains lysines that are positioned much like the $PI(4,5)P_2$ binding motif in cortexillin, where every fifth position after lysine was occupied by another lysine. This binding motif has also been suggested to be involved in $PI(4,5)P_2$ binding for cortexillin [57]. Two lysine residues (K43 and K46) of the putative $PI(4,5)P_2$ binding motif are located quite far from K38 and K51 in the three-dimensional structure (on the loop between β-strand C and D) and do not show significant CSP in the presence of $Ins(1,4,5)P_3$. However, considering the flexibility of unstructured region (K43–D53), the role of K43 and K46 cannot be ruled out in the case of $PI(4,5)P_2$ interactions. Interestingly, this predicted $PI(4,5)P_2$ binding motif of Palld-Ig3 does not belong to the previously identified actin binding basic patch (K15 and K18) [26]. The Palld-Ig3 domain has several lysine residues that are clustered on one face of the molecule (K13, K15, and K18), while another set of lysines (K36, K38, K43, K46, and K51) can be found on the opposite face of this β-sandwich structure [26]. Only three of these residues (K15, K18, and K51) have been shown to affect actin binding upon mutating to a neutral residue [26]. Interestingly, with the exception of K51, we did not observe any CSPs that were associated with residues involved in actin binding (K15 and K18). The previous study by Vattepu *et al.* (2014) reveals that Palld-Ig3 dimerization enhances actin crosslinking [35]. However, the residues of Palld-Ig3 involved in homodimerization have not been identified. We extend this finding with our results here that suggest that the $PI(4,5)P_2$-interacting cluster of Palld-Ig3 (K38–K51) may be involved in this dimerization surface, which would in turn would affect actin crosslinking. To test this hypothesis, we generated K38/51A mutation in Palld-Ig3. We observed that this mutation significantly reduced the *in vitro* actin crosslinking and polymerizing activity of Palld-Ig3 while only modestly lowering actin binding.

Our results are the first to indicate that two different regions in Palld-Ig3 are responsible for actin binding and bundling. Moreover, we also reveal that decreased bundling activity also affects *de novo* actin polymerization by palladin, perhaps by interfering with the stable palladin dimer. Our results also indicate a role for $PI(4,5)P_2$ regulation of palladin's activity via alteration of its actin crosslinking activity. $PI(4,5)P_2$ interferes with actin binding in many other ABPs, such as villin [52], vinculin [58], and cofilin [13], by competing with actin for overlapping binding sites. However, a similar mechanism for palladin regulation is not likely because this would result in the localization of palladin in the cytoplasm in the absence of actin, which is contrary to the established result of nuclear localization of palladin when the actin binding site is interrupted by mutagenesis [26]. This suggests that it is more plausible for the $PI(4,5)P_2$ to regulate palladin's activity via regulation of crosslinking activity rather than actin binding, and our data support this mode of regulation.

Materials and Methods

Expression and purification of palladin domains, palladin mutant (K38/51A), and actin

The *Mus musculus* Ig3, Ig4, and Ig34 domains of palladin were subcloned into the pTBSG (or pTBMalE) expression vector as described [35]. All constructs were transformed into BL21 (λDE3) *Escherichia coli* cells (New England Biolabs; Ipswich, MA) for protein expression. *E. coli* cultures were grown at 37 °C until the OD_{600} reached 0.7 and were

further grown overnight at 18 °C in ZYM-5052 auto-induction media as described [59]. Cell cultures were pelleted down and resuspended into lysis buffer [50 mM Tris (pH 8.0), 300 mM NaCl, and 10 mM imidazole], followed by sonication and clearing of cell lysate by centrifugation. Supernatant was loaded onto a pre-equilibrated Ni-NTA column, and protein was purified according to the manufacturer's guidelines (ThermoFisher Scientific; Waltham, MA). The N-terminal histidine tag was cleaved by TEV protease and further purified as previously reported [25]. Additionally, the MBP fusion protein was removed from the Palld-Ig34 construct by loading the TEV-digested Palld-Ig34 on amylose resin and was purified as per manufacturer's guidelines (New England Biolabs; Ipswich, MA). All three palladin domains were finally dialyzed in HBS buffer [20 mM Hepes (pH 7.4), 50 mM NaCl, and 1 mM DTT]. A double lysine point mutation (K38/51A) in the Palld-Ig3 domain was cloned in pQlinkH vector, and mutations were verified by sequencing. Palld-Ig3 K38/51A protein was purified as described for WT protein.

Uniform ^{15}N-isotopically labeled Palld-Ig3 was prepared by growing the *E. coli* cells in N-5052 auto-induction minimal media containing 10 mM $^{15}NH_4Cl$ (Sigma-Isotec, St. Louis, MO) as the sole nitrogen source [59]. Furthermore, Palld-Ig3 was purified as described for unlabeled protein and buffer exchanged into NMR buffer [20 mM Hepes (pH 6.9), 50 mM NaCl, 1 mM DTT, 0.05% NaN_3, and 10% D_2O].

Actin was purified from rabbit muscle acetone powder (Pel-Freez Biologicals; Rogers, AR) using the method described by Spudich and Watt [60] and was gel-filtered on 16/60 Sephacryl™ S-200 column (GE Healthcare Life Sciences). Purified G-actin was stored at 4 °C in G-buffer [5 mM Tris–HCl (pH 8), 0.1 mM $CaCl_2$, 0.2 mM DTT, 0.2 mM ATP, and 0.02% NaN_3] and was used within 1–2 weeks. Pyrene-labeled actin was prepared by the reaction of *N*-(1-pyrenyl) iodoacetamide (Sigma-Aldrich) with gel-filtered G-actin as described previously [49].

Preparation of phospholipid vesicles and vesicle co-sedimentation assay

POPC, L-α-PI (18:2), and L-α-PI(4)P (18:4; 1 mg/mL) dissolved in chloroform:methanol or chloroform were purchased from Avanti Polar Lipids, Inc. (Alabaster, AL, USA). PI(4,5)P_2 (diC8) in lyophilized form was purchased from Echelon Biosciences, Inc. (Salt Lake City, UT). A liposome co-sedimentation assay was carried out as described previously [36] to determine whether Palld-Ig3/Ig4/Ig34 interacts with POPC and PI(4,5)P_2. In brief, lipid vesicles of POPC with different ratios of PI(4,5)P_2 (5–20%) were made by mixing various quantities of PI(4,5)P_2 (12.5–50 μg) and POPC (237.5–200 μg). Lipid mixtures were then vacuum dried overnight and resuspended in HBS buffer before extensive sonication in a water bath for 15 min with highest power (model G112SPIT; Laboratory supplies, Inc. Hicksville, NY). Care was taken to keep the pH of lipid vesicles identical to the protein solutions. Similarly, lipid vesicles of POPC and PI/PI(4)P (15%) were prepared. Protein stock solutions of Palld-Ig3/Ig4/Ig34 were centrifuged at 100,000*g* for 50 min (Beckman TL-100 ultracentrifuge; Beckman-Coulter) to remove any protein aggregates. Liposomes of POPC and POPC/PI(4,5)P_2 were mixed with 10 μM Palld-Ig3/Ig4/Ig34 and incubated for 30 min before centrifugation at 100,000*g* for 40 min. The supernatants were removed, the pellet was resuspended in 100 μl of 0.1% SDS buffer [25 mM Tris (pH 8.3), 25 mM glycine, and

0.1% SDS], and the proteins in pellet and supernatant were separated using 10% tricine-SDS-PAGE gels. The amount of protein pelleted in each fraction was quantified by using ImageJ software [61]. At least three data sets were averaged, and SD was calculated. Further statistical analysis was done by one-way ANOVA test on GraphPad Prism software version 6 for Windows, (GraphPad Software, San Diego, California). Differences between values were considered significant if $P < 0.05$.

Tryptophan fluorescence quenching assay

Tryptophan fluorescence spectra of Palld-Ig3/Ig4/Ig34 were collected on a Cary-Eclipse spectrofluorometer (Varian, Agilent Technologies, Inc.). POPC vesicles (4 mM stock) were prepared for this experiment as described above, while 4 mM PI(4,5)P_2 micelle stock was prepared by resuspending PI(4,5)P_2 powder in HBS buffer, followed by sonication in water bath for 5 min. Palld-Ig3 (10 μM), Palld-Ig34 (10 μM), or Palld-Ig4 (20 μM) in HBS buffer was placed in a 1-cm square quartz cuvette with a sample volume of 200 μL at constant temperature of 25 °C. POPC vesicle or PI(4,5)P_2 micelles at final concentrations ranging from 2.5 μM to 70 μM were used in increments of 0.25 or 0.5 μL. Tryptophan fluorescence spectra were collected twice after 5 min of incubation at excitation wavelength of 295 nm and slit width of 5 nm for excitation and emission. The total volume of vesicle/micelles added did not exceed 2% of the initial protein solution at lower concentrations of POPC/PI(4,5)P_2. The decrease in fluorescence emission of Palld-Ig3 at 329 nm was plotted as a function of PI(4,5)P_2 concentration, and the change was assumed to be proportional to the concentration of protein–PI(4,5)P_2 complex. The apparent dissociation constant, K_d, for Palld-Ig3 and PI(4,5)P_2 was calculated using the Eq. (1) as described by Ward [62] and Lin [43],

$$\Delta F = \frac{\Delta F_{\max} \times [\text{lipid}_T]}{K_d + [\text{lipid}_T]} \quad (1)$$

where ΔF is the fluorescence quenching at a given PI(4,5)P_2 concentration, ΔF_{max} is the total fluorescence quenching of the protein saturated with ligand, and [lipid$_T$] is the concentration of PI(4,5)P_2. Data were fitted, and ΔF_{max} was determined for Palld-Ig3 and PI(4,5)P_2 binding by nonlinear regression analysis in GraphPad Prism version 7.

Actin crosslinking, co-polymerization, and pyrene fluorescence assay

Actin co-sedimentation assays were carried out to quantitate the effect of PI(4,5)P_2 on actin crosslinking by Palld-Ig3 that occurs during co-polymerization. PI(4,5)P_2 (0–150 μM) was incubated with 20 μM Palld-Ig3 for 30 min and was further incubated with Ca-G-actin in non-polymerizing conditions (G-buffer). The reaction mixtures were incubated for 1 h and then centrifuged at 5000*g* for 10 min. To pellet all actin filaments, we centrifuged the supernatant at 100,000*g* for 50 min. (Beckman TL-100 ultracentrifuge). Supernatant and pellet fractions were separated. All the fractions were resuspended in 100 μl of 0.1% SDS buffer that was further separated on 15% SDS-PAGE gels. The amount of Palld-Ig3 present in each fraction was quantified by using ImageJ software [61].

The actin co-sedimentation assay was adapted to determine the effect of $PI(4,5)P_2$ binding on the actin polymerizing activity of Palld-Ig3/Ig34. In these assays, Palld-Ig3/Ig34 (10 μM) was incubated with various amounts of $PI(4,5)P_2$ (0–150 μM) in HBS buffer with 1 mM EGTA for 30 min; thereafter, G-actin (10 μM) was added in non-polymerizing conditions (G-buffer) and further incubated for 1 h. To quantify the polymerized actin induced by $PI(4,5)P_2$-Palld-Ig3/Ig34, we centrifuged the reaction mixtures at 100,000*g* for 30 min. The supernatants were removed carefully, and the pellets were resuspended in 100 μl of 0.1% SDS buffer [25 mM Tris (pH 8.3), 25 mM glycine, and 0.1% SDS]. Pellet and supernatant fractions were further analyzed on 15% SDS-PAGE gels. The amount of actin polymerized in each sample was quantified by using ImageJ software [61].

To ascertain the effect of $PI(4,5)P_2$ on the rate of actin polymerization by Palld-Ig3, we measured the change in fluorescence intensity of 5% pyrenyl-actin, which is 7–10 times greater than the fluorescence intensity of G-actin as described [49]. Palld-Ig3 (20 μM) was mixed with various concentrations of $PI(4,5)P_2$ (20–100 μM) and incubated for 15 min at room temperature. Pyrenyl-G-actin and unlabeled G-actin were mixed together to make a 20-μM and 5% pyrene-labeled G-actin stock. Right before the experiment, 5 μM of this stock was incubated for 2 min upon the addition of 1 mM EGTA. Polymerization was then initiated by the addition of $PI(4,5)P_2$-Palld-Ig3/34 mixture with 25 mM KCl (polymerizing condition) to 5 μM G-actin. Pyrene fluorescence of actin was measured with excitation at 365 nm and emission at 385 nm in fluorescence spectrophotometer (PTI, Edison, New Jersey). We added equal amounts of storage buffer in the entire reaction sample to ensure that no contributions from Palld-Ig3 storage buffer affected polymerization. Baseline fluorescence was subtracted from the raw data. To determine the rate of overall polymerization, we first normalized the raw data by subtracting the baseline fluorescence and then dividing the fluorescence values by the steady-state plateau fluorescence. Then, the overall polymerization rate of each polymerization curve was determined by plotting the slope of the linear region of the curve and converting the relative fluorescence units/s into nM actin/s. We can assume that at equillibrium, the total amount of polymer is equal to the total concentration of actin minus the critical concentration, as Palld-Ig3 does not alter the critical concentration [34].

Similar experiments were done to determine the effect of Palld-Ig3 K38/51A mutation on actin polymerization. In brief, 5 μM pyrenyl-Ca-G-actin (5% labeled) was converted to Mg-G-actin by incubation in priming solution (1 mM EGTA and 0.1 mM $MgCl_2$) for 2 min. Palld-Ig3 K38/51A (0–20 μM) was added with 25 mM KCl to collect the fluorescence signal with instrument setting identical to previously described. Positive controls of WT Palld-Ig3/Ig34 were also recorded for each experimental condition. All fluorescence values were corrected for baseline fluorescence signal.

NMR chemical shift mapping of Palld-Ig3–Ins(1,4,5)P_3 complex

NMR spectra were collected on a Bruker Avance 800 MHz NMR instrument equipped with TCI cryoprobe and *Z*-axis pulsed field gradients at the University of Kansas Bio-NMR Lab. For the NMR experiments, the Palld-Ig3 solution was concentrated to 0.6 mM in NMR buffer. The $PI(4,5)P_2$ head group, $Ins(1,4,5)P_3$, in lyophilized form was purchased from

Echelon Biosciences, Inc., and 1 mg was dissolved in NMR buffer to make a 2-mM stock solution. 2D ^{15}N–^{1}H HSQC experiments were recorded for 0.2 mM Palld-Ig3 without and with Ins(1,4,5)P_3 (1 mM). Spectra were processed using NMRPipe [63] and analyzed by CARA [64]. CSPs were analyzed using CARA version 1.8.4, and combined CSPs with $\Delta\delta_{TOTAL}$ of $^{1}H_N$ and ^{15}N nuclei were weighted to normalize the larger chemical shift range of ^{15}N following the method as described by Williamson (2013) [65]:

$$\Delta\delta_{\mathrm{TOTAL}}(\mathrm{ppm})=\left[(\Delta\delta_{\mathrm{HN}})^2+(0.14\Delta\delta_{\mathrm{HN}})^2\right]^{1/2} \quad (2)$$

The cutoff of significance was measured by the mean value of the chemical shift difference (δ_{mean}); the 84 chosen residues were 22.9 ppb, and the SD (δ_{std}) was 19.5 ppb. The residues whose chemical shift changed by more than 41.4 ppb ($\delta_{mean} + \delta_{std}$) or 0.04 ppm were deemed significant CSPs [66].

Molecular docking

To validate the Ins(1,4,5)P_3 binding site onto the Palld-Ig3 domain, we performed the docking utilizing guru interface of HADDOCK2.2 [50] with 5000 structures for rigid-body docking. Palld-Ig3 coordinates used for the docking were extracted from the NMR structure of Palld-Ig3 (PDB ID: 2LQR) [26]. The ligand coordinates used for molecular docking were extracted from the X-ray crystal structure of the inositol 1,4,5-trisphosphate receptor binding core in complex with Ins(1,4,5)P_3 (PDB ID: 1N4K). HADDOCK2.2 docking of Ins(1,4,5)P_3 onto Palld-Ig3 resulted in a total of 198 conformers clustered in three groups that represented 99.0% of the water-refined models. All conformers were clusters according to their HADDOCK score, which is defined as a weighted sum of different energies ($1*E_{VDW} + 0.2E_{elec} + 0.1E_{AIR} + 1*E_{desolv}$). The results of the docking were visualized and analyzed by UCSF Chimera [67], WeNMR [68], and LIGPlOTv.4.5.3 [69].

Actin co-sedimentation assay and crosslinking assay of Palld-Ig3 K38/51A mutant

Actin co-sedimentation assays were carried out to quantitate the F-actin binding of Palld-Ig3 K38/51A mutant. In this assay, G-actin (10 μM) was polymerized into F-actin by the addition of polymerizing buffer [10 mM Tris (pH 7.5), 100 mM KCl, and 2 mM $MgCl_2$] for 40 min. Subsequently, it was incubated for 1 h with 10–40 μM Palld-Ig3K38/51A. This mixture of F-actin and protein was centrifuged at 100,000*g* for 50 min (Beckman TL-100 ultracentrifuge). To isolate the co-pelleted protein with F-actin, the supernatant was removed carefully and the pellet was resuspended in 100 μl of 0.1% SDS buffer and further separated on 15% SDS-PAGE gels. The amount of Palld-Ig3K38/51A present in each fraction was quantified by using ImageJ software [61], while Palld-Ig3 WT was used as positive control.

To quantitate the effect of Palld-Ig3K38/51A on actin crosslinking that occurs during co-polymerization, we incubated 10 μM Ca-G-actin with various amount of Palld-Ig3 (0–40 μM) in non-polymerizing conditions (G-buffer). Reaction conditions and sample analysis were done by following the protocol similar to the crosslinking of actin by Palld-Ig3 in the presence of PI(4,5)P_2.

Supplementary Material

Refer to Web version on PubMed Central for supplementary material.

Acknowledgments

We would like to thank Asokan Anbanandam and Justin Douglas, the Biomolecular NMR Laboratory managers at KU-COBRE Core facility at the University of Kansas, for their assistance in NMR data collection. The project was supported by a new investigator grant to M.R.B. from the Centers for Biomedical Research Excellence (COBRE) grant from the NCCR (5P20RR017708) and the NIGMS (8P20GM103420) and by an Institutional Development Award (IDeA) from the NIGMS of the NIH under grant number P20 GM103418.

Appendix A. Supplementary Data

Supplementary data to this article can be found online at http://dx.doi.org/10.1016/j.jmb.2016.07.018.

Abbreviations used

ABPs	actin binding proteins
CARA	computer-aided resonance assignment
PI(4,5)P_2	PI 4,5-bisphosphate
Palld-Ig3	Ig domain 3 of paladin
Ig	immunoglobulin
PI	phosphatidylinositol
PI(4)P	PI 4-phosphate
PI(3,4)P_2	PI 3,4-bisphosphate
ECM	extracellular matrix
HADDOCK2.2	High Ambiguity Driven protein–protein DOCKing
Ins(1,4,5)P_3	inositol trisphosphate
POPC	1-palmitoyl-2-oleoyl-sn-glycero-3-phosphocholine
HSQC	heteronuclear single quantum correlation spectroscopy
CSPs	chemical shift perturbations
G-actin	globular or monomeric actin
F-actin	filamentous actin
EGTA	ethylene glycol tetraacetic acid
HBS	HEPES buffered saline
MBP	maltose binding protein

N-WASP	Neural Wiskott-Aldrich syndrome protein
PC	phosphatidylcholine
PS	phosphatidylserine
WT	wild-type

References

1. Logan MR, Mandato CA. Regulation of the actin cytoskeleton by PIP_2 in cytokinesis. Biol Cell. 2006; 98:377–388. [PubMed: 16704377]
2. Hinchliffe K. Intracellular signalling: is PIP(2) a messenger too? Curr Biol. 2000; 10:R104–R105. [PubMed: 10679317]
3. Koch M, Holt M. Coupling exo- and endocytosis: an essential role for PIP(2) at the synapse. Biochim Biophys Acta. 1821; 2012:1114–1132.
4. Saarikangas J, Zhao H, Lappalainen P. Regulation of the actin cytoskeleton-plasma membrane interplay by phosphoinositides. Physiol Rev. 2010; 90:259–289. [PubMed: 20086078]
5. Yin HL, Janmey PA. Phosphoinositide regulation of the actin cytoskeleton. Annu Rev Physiol. 2003; 65:761–789. [PubMed: 12471164]
6. Higgs HN, Pollard TD. Activation by Cdc42 and PIP(2) of Wiskott–Aldrich syndrome protein (WASp) stimulates actin nucleation by Arp2/3 complex. J Cell Biol. 2000; 150:1311–1320. [PubMed: 10995437]
7. Sun H, Lin K, Yin HL. Gelsolin modulates phospholipase C activity *in vivo* through phospholipid binding. J Cell Biol. 1997; 138:811–820. [PubMed: 9265648]
8. Kusano K, Abe H, Obinata T. Detection of a sequence involved in actin-binding and phosphoinositide-binding in the N-terminal side of cofilin. Mol Cell Biochem. 1999; 190:133–141. [PubMed: 10098980]
9. Fraley TS, Tran TC, Corgan AM, Nash CA, Hao J, Critchley DR, et al. Phosphoinositide binding inhibits alpha-actinin bundling activity. J Biol Chem. 2003; 278:24,039–24,045.
10. Furuhashi K, Inagaki M, Hatano S, Fukami K, Takenawa T. Inositol phospholipid-induced suppression of F-actin-gelating activity of smooth muscle filamin. Biochem Biophys Res Commun. 1992; 184:1261–1265. [PubMed: 1317169]
11. Sechi AS, Wehland J. The actin cytoskeleton and plasma membrane connection: PtdIns(4,5)P(2) influences cytoskeletal protein activity at the plasma membrane. J Cell Sci. 2000; 113(Pt 21): 3685–3695. [PubMed: 11034897]
12. Raucher D, Stauffer T, Chen W, Shen K, Guo S, York JD, et al. Phosphatidylinositol 4,5-bisphosphate functions as a second messenger that regulates cytoskeleton-plasma membrane adhesion. Cell. 2000; 100:221–228. [PubMed: 10660045]
13. Gorbatyuk VY, Nosworthy NJ, Robson SA, Bains NP, Maciejewski MW, Dos Remedios CG, et al. Mapping the phosphoinositide-binding site on chick cofilin explains how PIP_2 regulates the cofilin–actin interaction. Mol Cell. 2006; 24:511–522. [PubMed: 17114056]
14. Ojala PJ, Paavilainen V, Lappalainen P. Identification of yeast cofilin residues specific for actin monomer and PIP_2 binding. Biochemistry. 2001; 40:15,562–15,569. [PubMed: 11141052]
15. Mykkanen OM, Gronholm M, Ronty M, Lalowski M, Salmikangas P, Suila H, et al. Characterization of human palladin, a microfilament-associated protein. Mol Biol Cell. 2001; 12:3060–3073. [PubMed: 11598191]
16. Luo H, Liu X, Wang F, Huang Q, Shen S, Wang L, et al. Disruption of palladin results in neural tube closure defects in mice. Mol Cell Neurosci. 2005; 29:507–515. [PubMed: 15950489]
17. Chang EH, Gasim AH, Kerber ML, Patel JB, Glaubiger SA, Falk RJ, et al. Palladin is upregulated in kidney disease and contributes to epithelial cell migration after injury. Sci Rep. 2015; 5:7695. [PubMed: 25573828]

18. Ronty MJ, Leivonen SK, Hinz B, Rachlin A, Otey CA, Kahari VM, et al. Isoform-specific regulation of the actin-organizing protein palladin during TGF-beta1-induced myofibroblast differentiation. J Invest Dermatol. 2006; 126:2387–2396. [PubMed: 16794588]
19. Najm P, El-Sibai M. Palladin regulation of the actin structures needed for cancer invasion. Cell Adhes Migr. 2014; 8:29–35.
20. Goicoechea SM, Garcia-Mata R, Staub J, Valdivia A, Sharek L, McCulloch CG, et al. Palladin promotes invasion of pancreatic cancer cells by enhancing invadopodia formation in cancer-associated fibroblasts. Oncogene. 2014; 33:1265–1273. [PubMed: 23524582]
21. Parast MM, Otey CA. Characterization of palladin, a novel protein localized to stress fibers and cell adhesions. J Cell Biol. 2000; 150:643–656. [PubMed: 10931874]
22. Liu XS, Luo HJ, Yang H, Wang L, Kong H, Jin YE, et al. Palladin regulates cell and extracellular matrix interaction through maintaining normal actin cytoskeleton architecture and stabilizing beta1-integrin. J Cell Biochem. 2007; 100:1288–1300. [PubMed: 17115415]
23. Jin L, Yoshida T, Ho R, Owens GK, Somlyo AV. The actin-associated protein palladin is required for development of normal contractile properties of smooth muscle cells derived from embryoid bodies. J Biol Chem. 2009; 284:2121–2130. [PubMed: 19015263]
24. Rachlin AS, Otey CA. Identification of palladin isoforms and characterization of an isoform-specific interaction between Lasp-1 and palladin. J Cell Sci. 2006; 119:995–1004. [PubMed: 16492705]
25. Dixon RD, Arneman DK, Rachlin AS, Sundaresan NR, Costello MJ, Campbell SL, et al. Palladin is an actin cross-linking protein that uses immunoglobulin-like domains to bind filamentous actin. J Biol Chem. 2008; 283:6222–6231. [PubMed: 18180288]
26. Beck MR, Dixon RD, Goicoechea SM, Murphy GS, Brungardt JG, Beam MT, et al. Structure and function of palladin's actin binding domain. J Mol Biol. 2013; 425:3325–3337. [PubMed: 23806659]
27. Boukhelifa M, Parast MM, Bear JE, Gertler FB, Otey CA. Palladin is a novel binding partner for Ena/VASP family members. Cell Motil Cytoskeleton. 2004; 58:17–29. [PubMed: 14983521]
28. Boukhelifa M, Moza M, Johansson T, Rachlin A, Parast M, Huttelmaier S, et al. The proline-rich protein palladin is a binding partner for profilin. FEBS J. 2006; 273:26–33. [PubMed: 16367745]
29. Ronty M, Taivainen A, Moza M, Otey CA, Carpen O. Molecular analysis of the interaction between palladin and alpha-actinin. FEBS Lett. 2004; 566:30–34. [PubMed: 15147863]
30. Ronty M, Taivainen A, Moza M, Kruh GD, Ehler E, Carpen O. Involvement of palladin and alpha-actinin in targeting of the Abl/Arg kinase adaptor ArgBP2 to the actin cytoskeleton. Exp Cell Res. 2005; 310:88–98. [PubMed: 16125169]
31. Ronty M, Taivainen A, Heiska L, Otey C, Ehler E, Song WK, et al. Palladin interacts with SH3 domains of SPIN90 and Src and is required for Src-induced cytoskeletal remodeling. Exp Cell Res. 2007; 313:2575–2585. [PubMed: 17537434]
32. Otey CA, Rachlin A, Moza M, Arneman D, Carpen O. The palladin/myotilin/myopalladin family of actin-associated scaffolds. Int Rev Cytol. 2005; 246:31–58. [PubMed: 16164966]
33. Goicoechea SM, Arneman D, Otey CA. The role of palladin in actin organization and cell motility. Eur J Cell Biol. 2008; 87:517–525. [PubMed: 18342394]
34. Gurung R, Yadav R, Brungardt JG, Orlova A, Egelman EH, Beck MR. Actin polymerization is stimulated by actin cross-linking protein palladin. Biochem J. 2016; 473:383–396. [PubMed: 26607837]
35. Vattepu R, Yadav R, Beck MR. Actin-induced dimerization of palladin promotes actin-bundling. Protein Sci. 2015; 24:70–80. [PubMed: 25307943]
36. Zhao H, Hakala M, Lappalainen P. ADF/cofilin binds phosphoinositides in a multivalent manner to act as a PIP(2)-density sensor. Biophys J. 2010; 98:2327–2336. [PubMed: 20483342]
37. Palmer SM, Playford MP, Craig SW, Schaller MD, Campbell SL. Lipid binding to the tail domain of vinculin: specificity and the role of the N and C termini. J Biol Chem. 2009; 284:7223–7231. [PubMed: 19110481]
38. Blin G, Margeat E, Carvalho K, Royer CA, Roy C, Picart C. Quantitative analysis of the binding of ezrin to large unilamellar vesicles containing phosphatidylinositol 4,5 bisphosphate. Biophys J. 2008; 94:1021–1033. [PubMed: 17827228]

39. McLaughlin SG, Szabo G, Eisenman G, Ciani SM. Surface charge and the conductance of phospholipid membranes. Proc Natl Acad Sci U S A. 1970; 67:1268–1275. [PubMed: 5274456]
40. Duex JE, Nau JJ, Kauffman EJ, Weisman LS. Phosphoinositide 5-phosphatase fig. 4p is required for both acute rise and subsequent fall in stress-induced phosphatidylinositol 3,5-bisphosphate levels. Eukaryot Cell. 2006; 5:723–731. [PubMed: 16607019]
41. Ceccon A, D'Onofrio M, Zanzoni S, Longo DL, Aime S, Molinari H, et al. NMR investigation of the equilibrium partitioning of a water-soluble bile salt protein carrier to phospholipid vesicles. Proteins. 2013; 81:1776–1791. [PubMed: 23760740]
42. Mercredi PY, Bucca N, Loeliger B, Gaines CR, Mehta M, Bhargava P, et al. Structural and molecular determinants of membrane binding by the HIV-1 matrix protein. J Mol Biol. 2016; 428:1637–1655. [PubMed: 26992353]
43. Lin KM, Wenegieme E, Lu PJ, Chen CS, Yin HL. Gelsolin binding to phosphatidylinositol 4,5-bisphosphate is modulated by calcium and pH. J Biol Chem. 1997; 272:20,443–20,450. [PubMed: 8995218]
44. Kim K, McCully ME, Bhattacharya N, Butler B, Sept D, Cooper JA. Structure/function analysis of the interaction of phosphatidylinositol 4,5-bisphosphate with actin-capping protein: implications for how capping protein binds the actin filament. J Biol Chem. 2007; 282:5871–5879. [PubMed: 17182619]
45. Maniti O, Khalifat N, Goggia K, Dalonneau F, Guerin C, Blanchoin L, et al. Binding of moesin and ezrin to membranes containing phosphatidylinositol (4,5) bisphosphate: a comparative study of the affinity constants and conformational changes. Biochim Biophys Acta. 1818; 2012:2839–2849.
46. Halaby DM, Poupon A, Mornon J. The immunoglobulin fold family: sequence analysis and 3D structure comparisons. Protein Eng. 1999; 12:563–571. [PubMed: 10436082]
47. Tatulian SA. Effect of lipid phase transition on the binding of anions to dimyristoylphosphatidylcholine liposomes. Biochim Biophys Acta. 1983; 736:189–195. [PubMed: 6652082]
48. Claessens MM, van Oort BF, Leermakers FA, Hoekstra FA, Cohen Stuart MA. Charged lipid vesicles: effects of salts on bending rigidity, stability, and size. Biophys J. 2004; 87:3882–3893. [PubMed: 15377511]
49. Cooper JA, Walker SB, Pollard TD. Pyrene actin: documentation of the validity of a sensitive assay for actin polymerization. J Muscle Res Cell Motil. 1983; 4:253–262. [PubMed: 6863518]
50. van Zundert GC, Rodrigues JP, Trellet M, Schmitz C, Kastritis PL, Karaca E, et al. The HADDOCK2.2 Web server: user-friendly integrative modeling of biomolecular complexes. J Mol Biol. 2016; 428:720–725. [PubMed: 26410586]
51. Goicoechea SM, Bednarski B, Garcia-Mata R, Prentice-Dunn H, Kim HJ, Otey CA. Palladin contributes to invasive motility in human breast cancer cells. Oncogene. 2009; 28:587–598. [PubMed: 18978809]
52. Kumar N, Zhao P, Tomar A, Galea CA, Khurana S. Association of villin with phosphatidylinositol 4,5-bisphosphate regulates the actin cytoskeleton. J Biol Chem. 2004; 279:3096–3110. [PubMed: 14594952]
53. Endlich N, Schordan E, Cohen CD, Kretzler M, Lewko B, Welsch T, et al. Palladin is a dynamic actin-associated protein in podocytes. Kidney Int. 2009; 75:214–226. [PubMed: 19116644]
54. von Nandelstadh P, Gucciardo E, Lohi J, Li R, Sugiyama N, Carpen O, et al. Actin-associated protein palladin promotes tumor cell invasion by linking extracellular matrix degradation to cell cytoskeleton. Mol Biol Cell. 2014; 25:2556–2570. [PubMed: 24989798]
55. Jin L, Kern MJ, Otey CA, Wamhoff BR, Somlyo AV. Angiotensin II, focal adhesion kinase, and PRX1 enhance smooth muscle expression of lipoma preferred partner and its newly identified binding partner palladin to promote cell migration. Circ Res. 2007; 100:817–825. [PubMed: 17322171]
56. Yu FX, Sun HQ, Janmey PA, Yin HL. Identification of a polyphosphoinositide-binding sequence in an actin monomer-binding domain of gelsolin. J Biol Chem. 1992; 267:14,616–14,621.

57. Stock A, Steinmetz MO, Janmey PA, Aebi U, Gerisch G, Kammerer RA, et al. Domain analysis of cortexillin I: actin-bundling, PIP(2)-binding and the rescue of cytokinesis. EMBO J. 1999; 18:5274–5284. [PubMed: 10508161]
58. Steimle PA, Hoffert JD, Adey NB, Craig SW. Polyphosphoinositides inhibit the interaction of vinculin with actin filaments. J Biol Chem. 1999; 274:18,414–18,420.
59. Studier FW. Protein production by auto-induction in high density shaking cultures. Protein Expr Purif. 2005; 41:207–234. [PubMed: 15915565]
60. Spudich JA, Watt S. The regulation of rabbit skeletal muscle contraction. I. Biochemical studies of the interaction of the tropomyosin–troponin complex with actin and the proteolytic fragments of myosin. J Biol Chem. 1971; 246:4866–4871. [PubMed: 4254541]
61. Abramoff MD, Magalhaes PJ, Ram SJ. Image processing with ImageJ. Biophoton Int. 2004; 11:36–42.
62. Ward LD. Measurement of ligand binding to proteins by fluorescence spectroscopy. Methods Enzymol. 1985; 117:400–414. [PubMed: 4079811]
63. Delaglio F, Grzesiek S, Vuister GW, Zhu G, Pfeifer J, Bax A. NMRPipe: a multidimensional spectral processing system based on UNIX pipes. J Biomol NMR. 1995; 6:277–293. [PubMed: 8520220]
64. Keller, RL. The Computer Aided Resonance Assignment Tutorial. 1st. Cantina Verlag; Zurich: 2004.
65. Williamson MP. Using chemical shift perturbation to characterise ligand binding. Prog Nucl Magn Reson Spectrosc. 2013; 73:1–16. [PubMed: 23962882]
66. Chen K, Bachtiar I, Piszczek G, Bouamr F, Carter C, Tjandra N. Solution NMR characterizations of oligomerization and dynamics of equine infectious anemia virus matrix protein and its interaction with PIP_2. Biochemistry. 2008; 47:1928–1937. [PubMed: 18220420]
67. Pettersen EF, Goddard TD, Huang CC, Couch GS, Greenblatt DM, Meng EC, et al. UCSF Chimera—a visualization system for exploratory research and analysis. J Comput Chem. 2004; 25:1605–1612. [PubMed: 15264254]
68. Wassenaar TA, van Dijk M, Loureiro-Ferreira N, van der Schot G, de Vries SJ, Schmitz C, et al. WeNMR: structural biology on the grid. J Grid Comput. 2012; 10:743–767.
69. Wallace AC, Laskowski RA, Thornton JM. LIGPLOT: a program to generate schematic diagrams of protein–ligand interactions. Protein Eng. 1995; 8:127–134. [PubMed: 7630882]

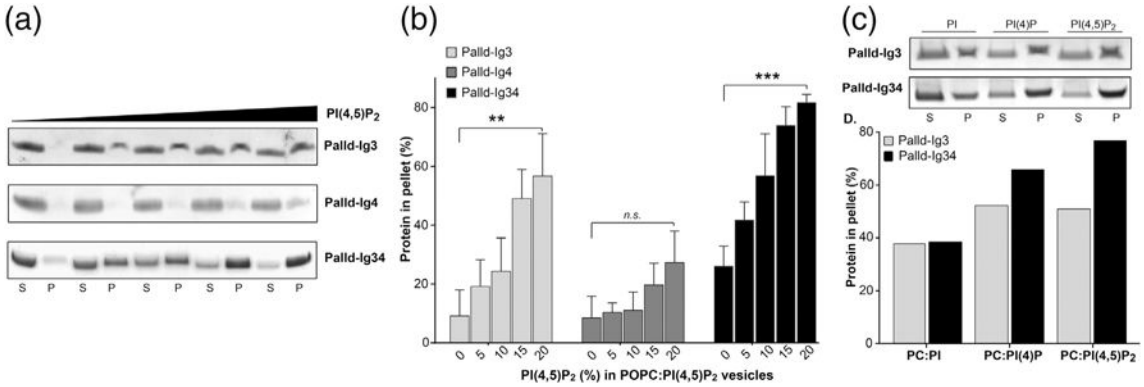

Fig. 1.

Influence of lipid constituents on Palld-Ig3/4/34 domains binding to liposomes determined by co-sedimentation. (a.) Indicated proteins with different concentrations of $PI(4,5)P_2$ (5–20%) in PC vesicles were incubated and centrifuged. Supernatant (S) and pellet (P) fractions obtained were separated on tricine-SDS gels. Representative gels from one of the three independent experiments are shown. (b.) Quantitative representation of (a), where the amount of indicated protein in supernatant and pellet was quantified from the relative band intensity on the gel. Three independent experiments were performed; error bars indicate SD. Significance tested by one-way ANOVA test: **, $P < 0.001$; ***, $P < 0.0001$; n.s., non-significant. (c.) Indicated proteins (10 μM) were incubated with POPC vesicle enriched with 15% PI, PI(4)P, or $PI(4,5)P_2$ lipids and were centrifuged. Supernatant (S) and pellet (P) fractions obtained and separated on tricine-SDS gels and the representative gels are shown. (d.) Quantitative representation of (c), where the amount of indicated protein in supernatant and pellet was quantified as reported earlier.

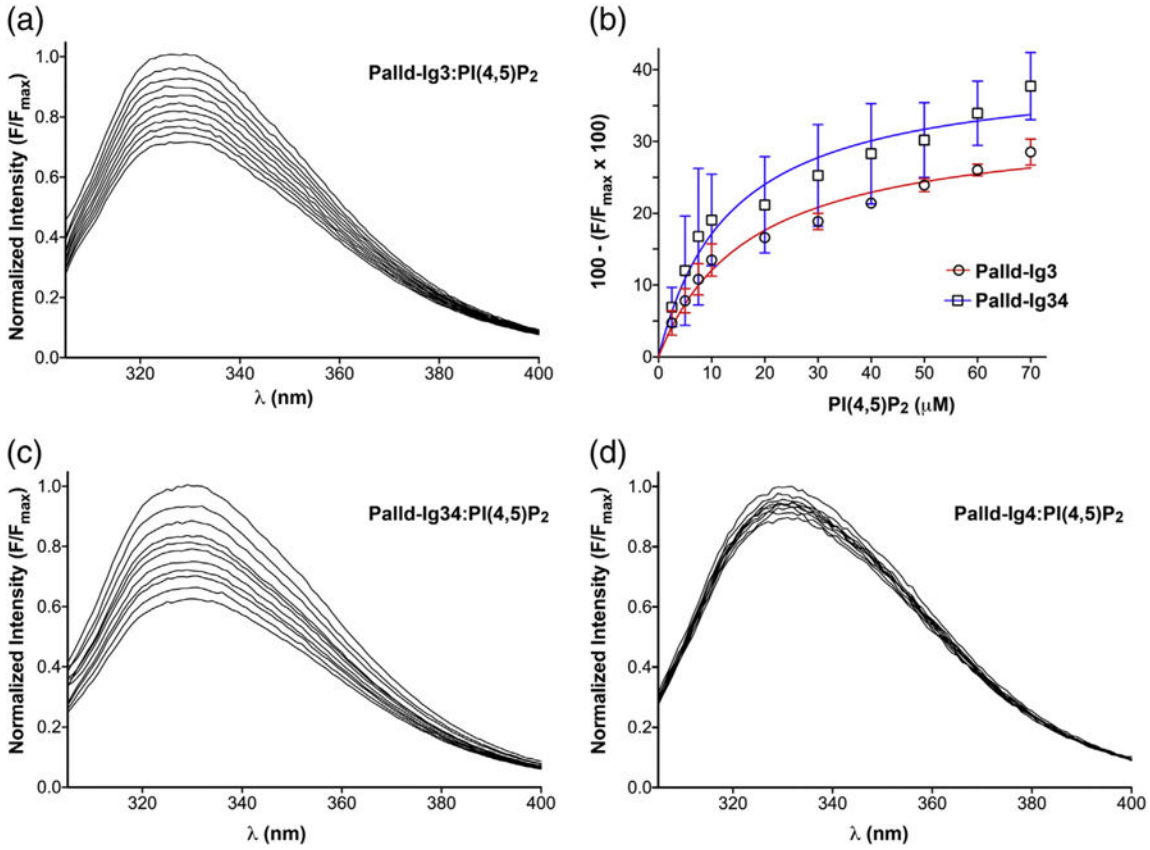

Fig. 2.

Binding affinity assessed by quenching of fluorescence. (a, c, and d) $PI(4,5)P_2$ (0–70 μM from 4 mM stock solution) was sequentially added to Palld-Ig3/4/34 and the quenching of intrinsic tryptophan fluorescence. The observed intensity was normalized by dividing each data point with the fluorescence intensity of protein without $PI(4,5)P_2$ and was plotted against wavelength. Analysis of binding of Palld-Ig3 and Ig34 with $PI(4,5)P_2$ was done by plotting $100-(F/F_{max}\times 100)$ against $PI(4,5)P_2$ concentration. (b) Data points were fitted to the experimental data with nonlinear curvefit program in Prism GraphPad. The apparent dissociation constant (K_d) for Palld-Ig3 and Ig34 with $PI(4,5)P_2$ was found to be similar (17.3 ± 2.1 and 13.5 ± 4 μM, respectively) for this experiment. Three separate experiments were performed and error bars indicate SD.

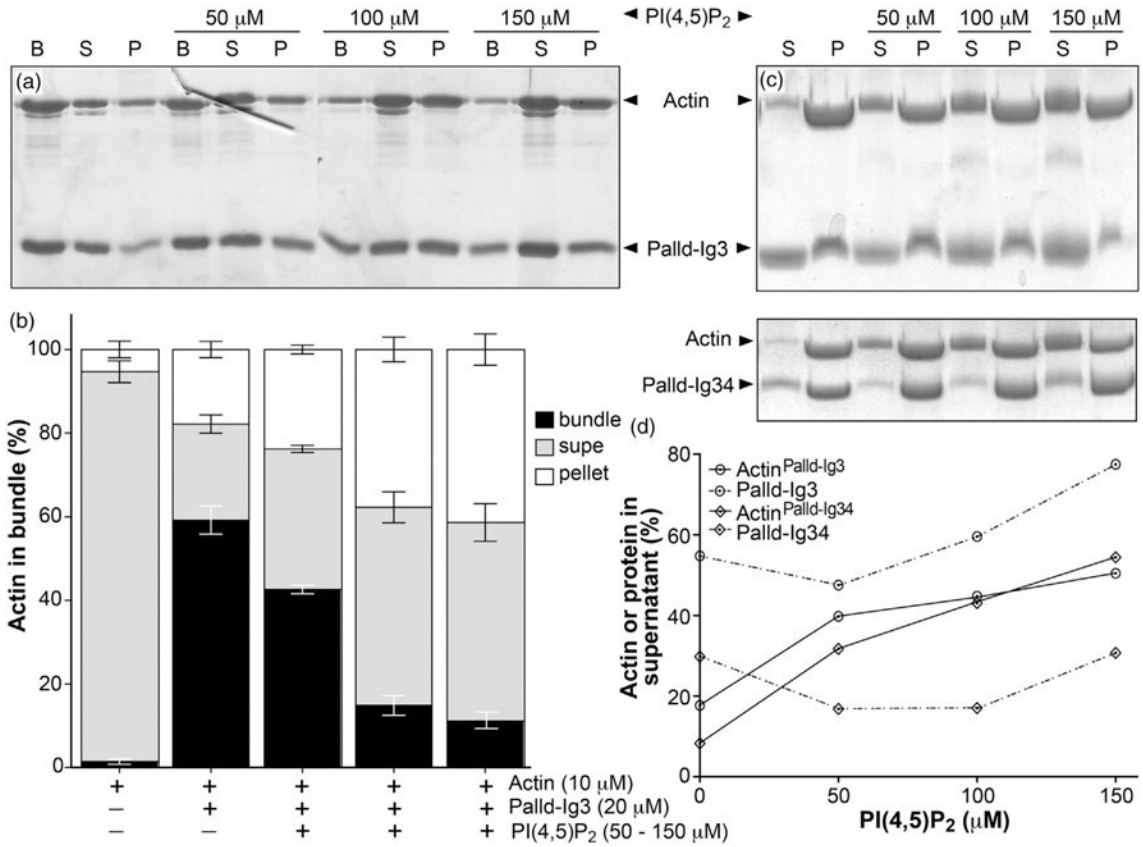

Fig. 3.

Interactions with $PI(4,5)P_2$ affect actin crosslinking and polymerizing activity of palladin. (a) A differential centrifugation assay was used to assess the effect of $PI(4,5)P_2$ (0–150 μM) on Palld-Ig3's (20 μM) ability to crosslink actin (10 μM) in G-buffer condition. Samples were subjected to low-speed centrifugation, and crosslinked actin filaments (b) were obtained before sedimenting the remaining F-actin by ultracentrifugation and resolving the supernatant (S) and pellet (P) from these spins by SDS-PAGE. Representative gels from one of the three independent experiments are shown. (b) Quantification of actin crosslinking was analyzed by densitometry of the actin bands to estimate the effect of $PI(4,5)P_2$. The percentage of actin found in the low-speed bundle is represented by the black bar; soluble portion is gray and high-speed pelleted actin is white. Three separate experiments were performed and error bars indicate SD (c) Representative SDS-PAGE gels of co-sedimentation assay of actin and mixture of protein:lipid (Palld-Ig3/34:$PI(4,5)P_2$) in G-buffer conditions. Palld-Ig3/34 (10 μμ) was incubated for 30 min with $PI(4,5)P_2$ (0–150 μμ) and this mixture was further incubated with G-actin (10 μμ) in G-buffer condition for 1 h. Supernatant (S) and pellet (P) fractions were separated by centrifugation. (b.) Supernatant fraction of Palld-Ig3/34 protein and unpolymerized G-actin was quantified from relative band intensity on the gel and plotted against $PI(4,5)P_2$ concentration.

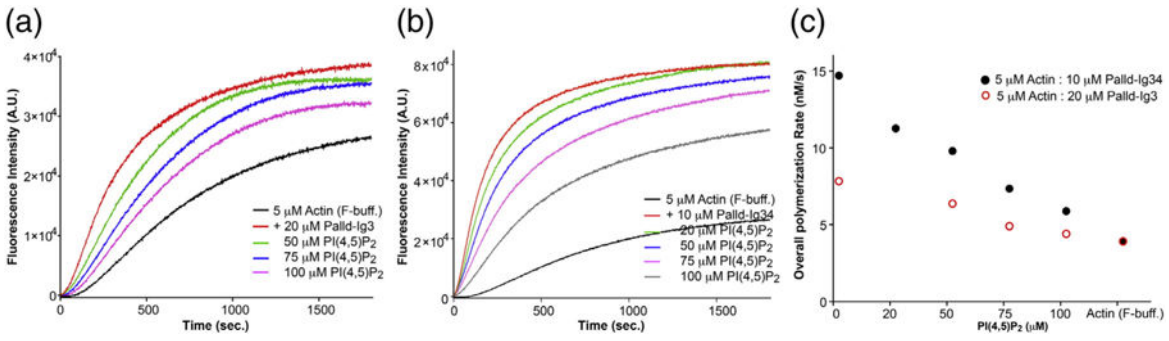

Fig. 4. In vitro

actin polymerization assays show that binding of Palld-Ig3/34 to PI(4,5)P_2 decreases its actin polymerizing activity. Spontaneous assembly reactions were performed by the addition of 5 μM actin (5% pyrene labeled with 1 mM EGTA) and 20 μM Palld-Ig3 (a) or 10 μM Palld-Ig34 (b) with increasing concentrations of the PI(4,5)P_2 (0–100 μM) in F-buffer (25 mM KCl). (c) Plots of overall polymerization rate (nM/s) *versus* PI(4,5)P_2 concentration for Palld-Ig3 and Ig34 in the binding of PI(4,5)P_2 with Palld-Ig3 or Ig34 decrease the rate of actin polymerization in F-buffer conditions.

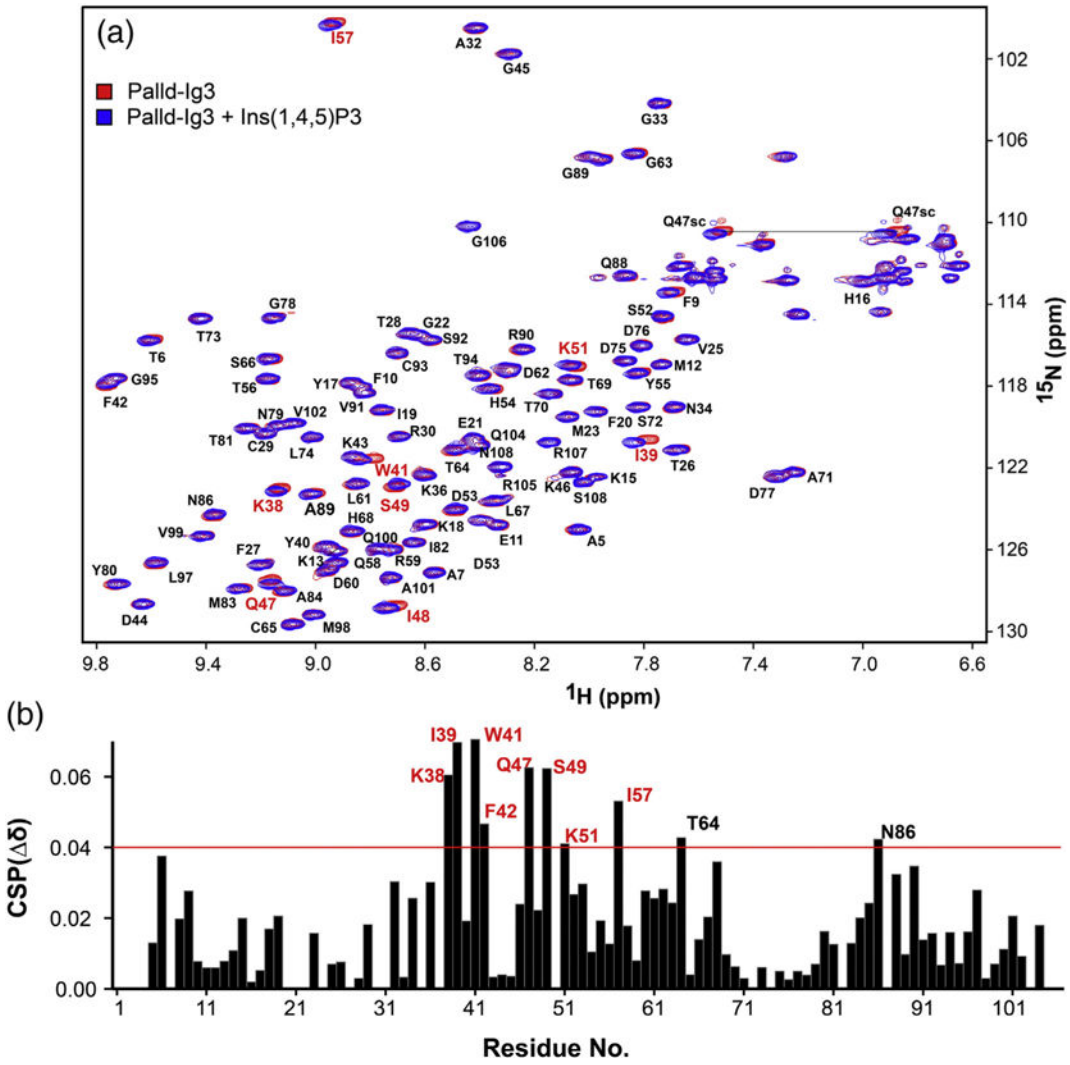

Fig. 5.

Mapping of Ins(1,4,5)P_3 binding region on Palld-Ig3 by CSP measurment. (a) Overlay of ^{1}H–^{15}N HSQC spectra of 0.2 mM Palld-Ig3 with (blue) and without (red) 1 mM Ins(1,4,5)P_3. Peaks showing significant CSP are highlighted with red. (b) CSPs for Palld-Ig3 and Ins(1,4,5)P_3 interaction were calculated and plotted against the residue number. A CSP cutoff of 0.04 ppm was considered as significant.

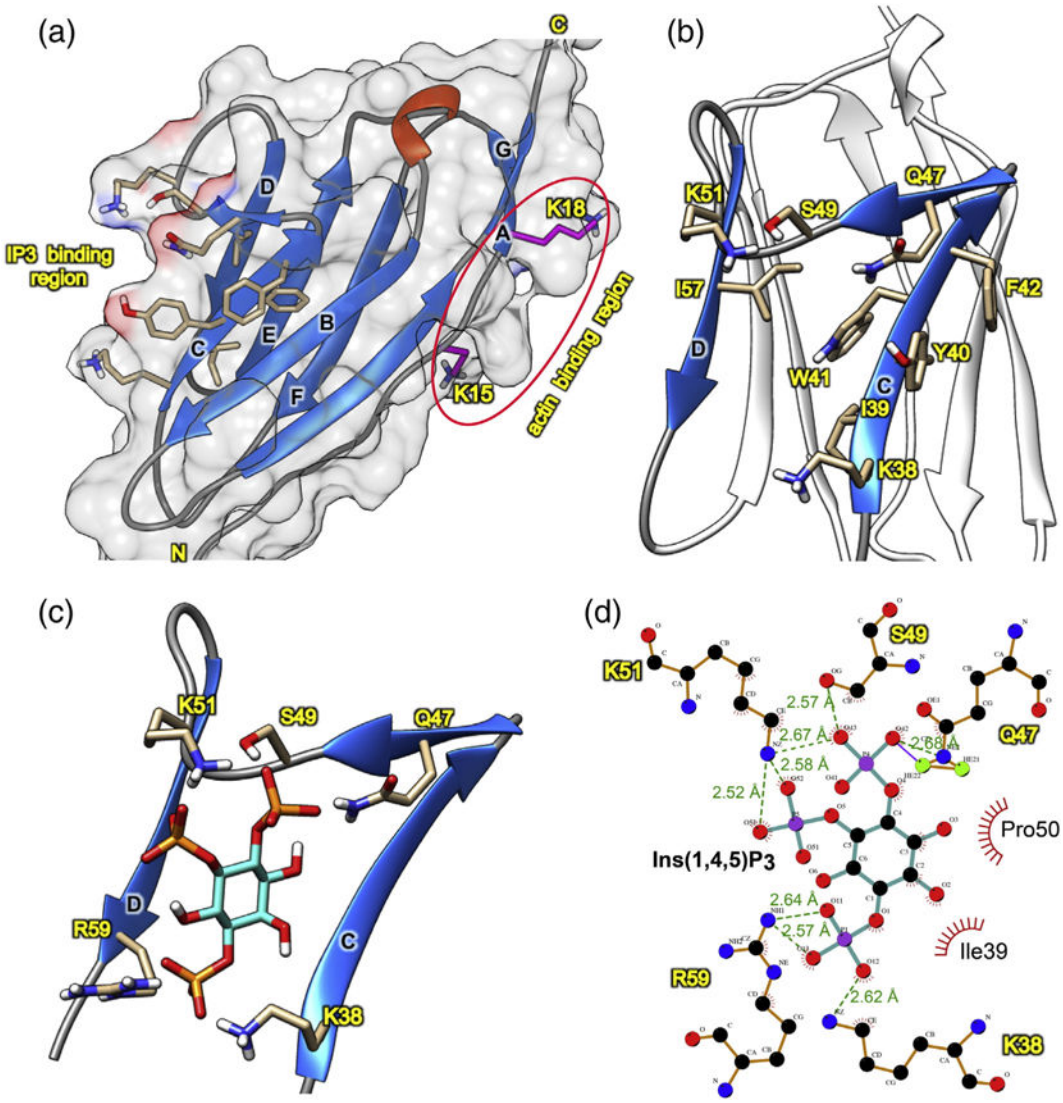

Fig. 6.

Mapping of Ins(1,4,5)P_3 binding region on Palld-Ig3 structure and docking model for Palld-Ig3:Ins(1,4,5)P_3 complex. (a) Residues showing significant CSPs upon binding to Ins(1,4,5)P_3 are highlighted by stick representation (light brown) onto the structure of Palld-Ig3 (PDB ID: 2LQR), and known actin binding residues are marked and shown in magenta. (b) The proposed Ins(1,4,5)P_3 binding region is zoomed in to show the highlighted residues clustered on the β-strand C and D and the loop in between. (c) The representative docking model of Palld-Ig3:Ins(1,4,5)P_3 with the highest HADDOCK score resulted from HADDOCK docking and was visualized by UCSF Chimera [67]. Side chains of the residues involved in the binding model are represented in stick (light brown), and Ins(1,4,5)P_3 carbon ring is colored in cyan. (d) Stick representation of Palld-Ig3:Ins(1,4,5)P_3 interface as analyzed by LIGPLOTv.4.5.3 [6969]. Ins(1,4,5)P_3 carbon ring is colored in cyan, and the hydrogen bond between ligand and protein is shown in green color.

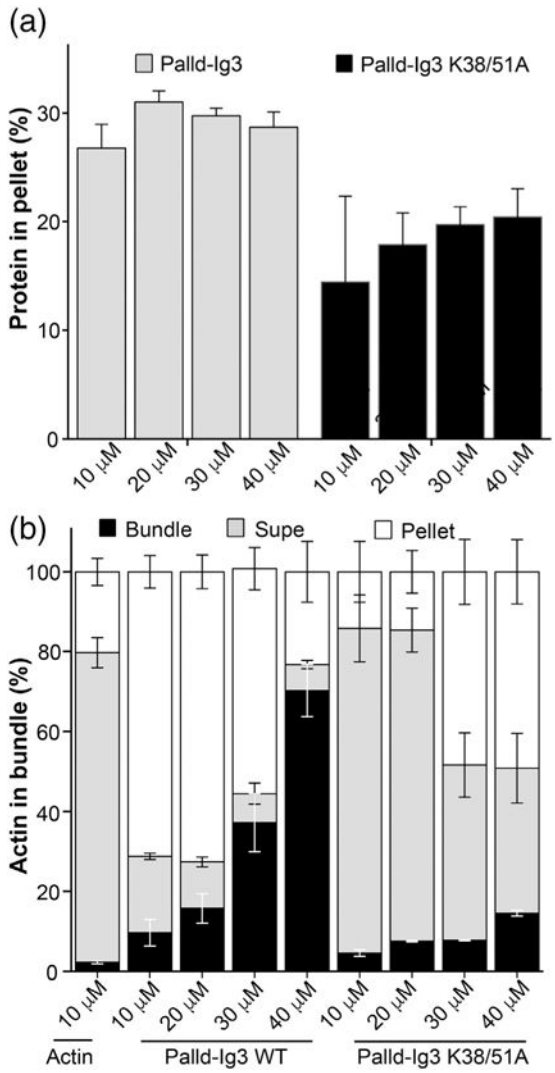

Fig. 7.

Actin binding and crosslinking activity reduced by double mutation (K38/51A) of Palld-Ig3. (a) Quantitative analysis of the amount of WT Palld-Ig3 and mutant bound to F-actin. For all co-sedimentation assays, various concentrations of palladin protein (10–40 μM) were incubated with 10 μM actin. Each experiment was repeated three times with SD error bars shown. (b) Differential centrifugation assay was used to assess the crosslinking in G-buffer condition by Palld-Ig3 K38/51A mutant and was compared with WT Palld-Ig3. Quantification of actin crosslinking was analyzed by densitometry of the actin bands to estimate the ability of various palladin mutant and WT concentrations to crosslink actin. In all of these assays, the concentration of actin was held constant at 10 μM, and the WT and mutant were varied from 10 μM to 40 μM. The percentage of actin found in the low-speed bundle is represented by the black bar; soluble portion is gray and high-speed pelleted actin is white. Three separate experiments were performed and error bars indicate SD.

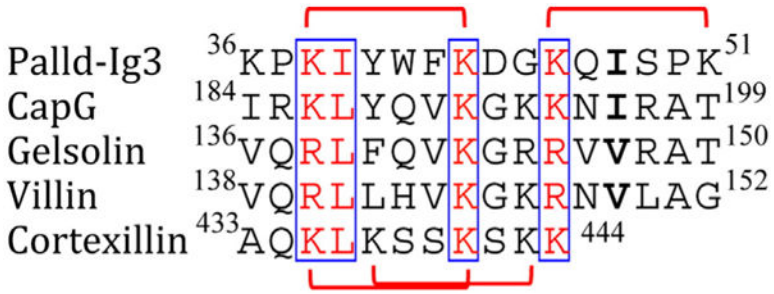

Fig. 8.

Sequence alignment of Palld-Ig3 (residues 36–51) and PI(4,5)P_2 binding motif from various ABPs. The consensus sequence for the PI(4,5)P_2 binding motif is R/K-$(X)_4$-[R/K]-X-[RR/KK]. Boxes indicate identical or conservatively substituted residues among the aligned PI(4,5)P_2 binding proteins. The numbers of the first and last residues of the aligned sequences are given. Bridging brackets between lysines in Palld-Ig3 and cortexillin reveal the pattern of lysines at every fifth residue.